Remanence and coercivity in isotropic nanocrystalline permanent magnets

T. Schrefl
Institut für Angewandte und Technische Physik, T.U. Wien, Wiedner Hauptstrasse 8, A-1040 Vienna, Austria and Max-Planck-Institut für Metallforschung, Institut für Physik, Postfach 80 06 65, 70506 Stuttgart, Germany

J. Fidler
Institut für Angewandte und Technische Physik, T.U. Wien, Wiedner Hauptstrasse 8, A-1040 Vienna, Austria

H. Kronmüller
Max-Planck-Institut für Metallforschung, Institut für Physik, Postfach 80 06 65, 70506 Stuttgart, Germany
(Received 7 July 1993; revised manuscript received 23 August 1993)

Numerical micromagnetic calculations rigorously describe the correlation between the microstructure and the magnetic properties of nanocrystalline permanent magnets. In isotropic nanocrystalline permanent magnets exchange interactions override the anisotropy of the individual grains. Therefore the spontaneous magnetic polarization deviates from the easy axes in a region along the grain boundaries. For a fine grain structure with a mean grain size $d < 20$ nm the remanence is considerably enhanced, since the volume fraction of the boundary regions where the spontaneous magnetic polarization points towards the direction of the applied field becomes significantly high. The inhomogeneous ground state, however, favors the nucleation of reversed domains leading to a reduction of the coercive field with decreasing grain size. A uniform grain structure with a very small range in grain size avoids large demagnetizing fields and thus preserves a high coercivity. For a grain size of 10 nm isotropic two-phase permanent magnets based on $Fe_{14}Nd_2B$ and α-Fe show remarkable high-energy products, because the volume fraction of the magnetically soft phase can be increased up to 50% without a significant loss of coercivity.

I. INTRODUCTION

The interplay between the intrinsic magnetic properties and the microstructure determines both remanence and coercivity of permanent magnets. As a consequence the magnetic behavior of permanent magnets depends sensitively on microstructural properties such as grain size, particle shape, grain boundary type, and the distribution of magnetically hard and soft phases. In order to obtain high-energy products, it is necessary to increase the remanence and keep the coercive field sufficiently high.[1] McCallum *et al.*[2] reported an enhanced remanence in melt-spun Nd-Fe-B magnets being composed of nanocrystalline homogeneous grains without any nonmagnetic phases separating adjacent grains. A further increase of the remanence is possible in nanostructured two-phase systems where small soft magnetic grains of high spontaneous magnetization such as α-Fe are strongly exchange coupled to a hard magnetic phase. Coehoorn, Mooij, and Waard[3] found remarkable high-energy products in melt-spun permanent magnets of nominal composition containing a substantial fraction of Fe_3B grains. Recently, Ding, McCormick, and Street[4] reported a maximum energy product of more than $(BH)_{max} = 200$ kJ/m^3 in mechanically alloyed, isotropic Sm_7Fe_{93}-nitride powders where exchange interactions between a soft α-Fe and a hard magnetic $Sm_2Fe_{17}N_x$ phase cause a significant enhancement of the remanence.

For nanocrystalline permanent magnets without any nonmagnetic phases separating adjacent grains the ratio of the remanent polarization J_r to the saturation polarization J_s exceeds the theoretical limit 0.5,[5,6] given by the Stoner-Wohlfarth theory.[7] For noninteracting uniaxial single domain particles the remanent magnetic polarization is given by[2]

$$J_r = J_s\langle\cos\theta\rangle, \tag{1}$$

where θ is the angle between the easy axes and the saturation field and $\langle\ \rangle$ denotes an ensemble average. According to (1) J_r/J_s is 0.5 for an assembly of noninteracting and randomly oriented particles, whereas J_r/J_s is $2/\pi = 0.637$ for microstructures with in-plane random texture. In general, remanence enhancement is attributed to intergrain exchange interactions.[5] Exchange interactions between neighboring grains cause the spontaneous magnetic polarization to deviate from the easy axes. As a consequence the resultant polarization parallel to the direction of the applied field is increased. In two-phase permanent magnets remanence enhancement owing to exchange interactions is much more effective: Almost all the magnetic moments of the soft phase are aligned parallel to the direction of the saturation field, which corresponds to the average direction of the easy axes of the neighboring hard magnetic grains.[8]

In addition to the remanence, the coercive field of permanent magnets strongly depends on intergrain interac-

tions and thus on microstructural parameters. Since exchange coupling of neighboring grains favors the nucleation of reversed domains,[9,10] remanence enhancement is generally achieved at the expense of coercivity. In nanocrystalline isotropic magnets which show an enhanced remanence the coercive field considerably drops with decreasing grain size.[11] Two-phase permanent magnets show remarkable high coercivities if the size of soft magnetic grains is sufficiently small.[1]

A theoretical treatment of these phenomena must take into account interactions of the grains. Callen, Liu, and Cullen[12] used a molecular field approximation to describe intergrain interactions in amorphous ferromagnets. As shown by Hadjipanayis and Gong[6] this model can describe the relation between remanence and coercivity found in Nd-Fe-Al-B-Si magnets. Fukunaga and Inoue[13] numerically investigated the effect of intergrain exchange and magnetostatic interactions on remanence and coercivity for an isotropic model magnet composed of cubic particles. The results show that intergrain exchange interactions increase the remanence and reduce the coercive field of isotropic magnets. Magnetostatic interactions were found to be negligible. Using a one-dimensional micromagnetic model, Kneller and Hawig[1] estimated the critical dimensions of the phases and derived the magnetic properties of two-phase permanent magnets. The optimum microstructure was found to consist of hard grains embedded in a magnetically soft matrix with lateral dimensions of both phases about equal to the domain wall width of the hard phase.

Whereas nucleation fields can be explicitly derived for multilayers being composed of magnetically soft and hard layers,[14,15] a quantitative treatment of the correlation between the microstructure and the magnetic properties in isotropic permanent magnets requires numerical and computational techniques. In this study the dependence of the remanence and the coercive field on the mean grain size, the shape of the grains, and the distribution of magnetically hard and soft phases has been numerically investigated using a finite element technique. We consider a two-dimensional grain structure where the easy axes of the particles lie within a plane. The magnetization is constrained to this plane and taken to be uniform in the direction perpendicular to the plane. Despite the restriction to two-dimensional microstructures the presented numerical model rigorously describes the magnetic behavior of real magnets.

(1) The nonlinear micromagnetic problem is solved for a realistic two-dimensional microstructure without any further approximations. The influence of characteristic features of the microstructure such as size and shape of the grains can be treated quantitatively.

(2) Particle interactions are an inherent part of the simulation model. The model takes into account both, short-range exchange and long-range magnetostatic interactions.

(3) The magnetic moments may become inhomogeneously arranged within a grain. Thus it is possible to calculate the distribution of the magnetic polarization at the grain boundaries which was found to influence the magnetic properties significantly.

(4) Magnetic stray fields arising from magnetic surface charges at the boundaries between magnetically soft and hard grains and from magnetic volume charges owing to an inhomogeneous distribution of the spins within the grains are taken into account.

Reference calculations for three-dimensional particles and micromagnetic energy considerations show that the magnetic behavior of melt-spun Nd-Fe-B magnets can be reasonably described by two-dimensional micromagnetic calculations. The restriction to planar magnetization processes overapproximates the stray field energy and thus leads to smaller nucleation fields as compared to the three-dimensional case. Micromagnetic calculations for two interacting hard magnetic particles show that the nucleation field of dodecahedral particles and infinitely extended hexagonal prisms with similar easy axes configuration and equivialent diameters differ by less than 10%.[16] In three dimensions, curlinglike rotations of the magnetization can always reduce the stray field energy. The energy gain owing to magnetization curling is small as compared to the contributions of the magneticrystalline anisotropy energy and of the exchange energy which dominate the magnetization process in small-grained, isotropic Nd-Fe-B magnets. Fukunaga and Inoue[13] showed that magnetostatic interactions do not considerably influence the magnetic behavior of isotropic Nd-Fe-B magnets. Whereas the curlinglike magnetic states which are possible in three dimensions reduce the stray field energy, the exchange energy arising at the interface between misoriented neighboring grains will be the same for planar and curling magnetization processes. Therefore it will be sufficient to consider two-dimensional microstructures, in order to describe the magnetic properties of nanocrystalline isotropic Nd-Fe-B magnets.

Since the simulation method relies only on micromagnetic concepts and does not introduce any artificial assumptions, the numerical results help to understand the effects of microstructural features on remanence and coercivity within the framework of micromagnetism. Section II of this paper describes the micromagnetic background of the simulation model. Section III presents numerical results for the size dependence of remanence and coercivity. Section IV deals with the influence of the particle shape on the coercive field. The results presented in Sec. V show the effects of the grain size and of the distribution of magnetically hard and soft phases on the magnetic properties of two-phase exchange hardened permanent magnets.

II. MICROMAGNETIC BACKGROUND

A theoretical treatment of magnetization processes starts form the magnetic Gibbs free energy, ϕ_t, which is composed of the exchange energy, the magnetocrystalline energy, the stray field energy, and the magnetostatic energy of the spontaneous magnetic polarization, $\boldsymbol{J}_s$, in an external field, $\boldsymbol{H}_{\text{ext}}$. The minimization of the total Gibbs free energy with respect to $\boldsymbol{J}_s$, subject to

the constraint $|\boldsymbol{J}_s| = J_s$, provides a stable equilibrium state of a magnetic structure. We assume a geometry where the easy axes of the grains as well as the magnetization are constrained to a plane. The magnetization is taken to be uniform in the direction perpendicular to this plane. In other words, the grains are infinitely extended in the direction that is perpendicular to all easy axes. Because of translational symmetry along the direction perpendicular to the plane containing the easy axes, only processes in this plane need to be considered. For this two-dimensional geometry ϕ_t depends only on the angle φ between $\boldsymbol{J}_s$ and the easy axis and is given by[17,18]

$$\phi_t = \int \left\{ A\left[\nabla\varphi(\boldsymbol{r})\right]^2 + K_1 \sin^2\varphi(\boldsymbol{r}) + K_2 \sin^4\varphi(\boldsymbol{r}) - (1/2)\boldsymbol{H}_s(\boldsymbol{r})\cdot\boldsymbol{J}_s(\boldsymbol{r}) - \boldsymbol{H}_{\text{ext}}\cdot\boldsymbol{J}_s(\boldsymbol{r}) \right\} d^2r, \tag{2}$$

where K_1, K_2 are the anisotropy constants, and A is the exchange constant. The demagnetizing field $\boldsymbol{H}_s$, whose source is $\boldsymbol{J}_s$, couples the micromagnetic problem with Poisson's equation for the magnetic scalar potential: The demagnetizing field $\boldsymbol{H}_s$ follows from a magnetic scalar potential $U(\boldsymbol{r})$ by $\boldsymbol{H}_s = -\nabla U(\boldsymbol{r})$, where $U(\boldsymbol{r})$ obeys Poisson's equation

$$\triangle U(\boldsymbol{r}) = \nabla\cdot\boldsymbol{J}_s \tag{3}$$

with the solution

$$U(\boldsymbol{r}) = \frac{1}{2\pi\mu_0}\int \ln|\boldsymbol{r}-\boldsymbol{r}'|\,\nabla\cdot\boldsymbol{J}_s\,d^2r' - \frac{1}{2\pi\mu_0}\int \ln|\boldsymbol{r}-\boldsymbol{r}'|\,\boldsymbol{J}_s\cdot\boldsymbol{n}\,df'. \tag{4}$$

Here the first term takes care of the magnetic volume charges $\nabla\cdot\boldsymbol{J}_s$ within the grains and the second term of magnetic surface charges $\boldsymbol{J}_s\cdot\boldsymbol{n}$ ($\boldsymbol{n}$ denotes the surface normal) at the grain boundaries.

Numerical micromagnetic calculations either minimize (2) directly[19,20] or solve the corresponding system of simultaneous differential equations.[21] For the numerical calculation of the stray field energy it is worthwhile to consider two magnetostatic theorems. Brown[22] showed that the stray field energy ϕ_s due to $\boldsymbol{J}_s(\boldsymbol{r})$ can be approximated by lower and upper bounds, given by

$$\phi_s \geq W_1[\boldsymbol{J}_s, U] = \int \nabla U\cdot\boldsymbol{J}_s\,d^3r - \frac{\mu_0}{2}\int (\nabla U)^2\,d^3r, \tag{5}$$

$$\phi_s \leq W_2[\boldsymbol{J}_s, \boldsymbol{A}] = \frac{1}{2\mu_0}\int (\nabla\times\boldsymbol{A} - \boldsymbol{J}_s)^2\,d^3r, \tag{6}$$

where U is an arbitrary function of space which is continuous and regular at infinity, and $\boldsymbol{A}$ is an arbitrary continuous vector whose derivatives are also continuous everywhere. Both U and $\boldsymbol{A}$ need not be related to $\boldsymbol{J}_s$. If maximized with respect to U, W_1 reduces to the stray field energy ϕ_s and makes U equal to the actual magnetic scalar potential, $-\nabla U = \boldsymbol{H}_s$. The Euler-Lagrange equation which results from the variation of the functional W_1 with respect to U is Poisson's equation (3) for the magnetic scalar potential. Replacing the stray field energy ϕ_s in the total magnetic Gibbs free energy by W_1 one obtains an auxiliary functional $\bar{W}[\boldsymbol{J}_s, U]$ whose stationary points correspond to the stationary points of the total magnetic Gibbs free energy.[23] All stationary points of $\bar{W}$ are saddle points,[24,23] which complicates the numerical search for equilibrium states. Generally, iterative numerical micromagnetic algorithms which alternate between solving Poisson's equation for fixed $\boldsymbol{J}_s$ and minimizing Gibbs free energy for fixed demagnetizing field proceed towards a saddle point of $\bar{W}$. A process of iterating towards a maximum with respect to U and towards a minimum with respect to $\boldsymbol{J}_s$ may easily lead to convergence difficulties.[19]

On the other hand, replacing ϕ_s in the magnetic Gibbs free energy by $W_2[\boldsymbol{J}_s, \boldsymbol{A}]$ leads to an auxiliary functional $W[\boldsymbol{J}_s, \boldsymbol{A}]$ whose local minima are in one-to-one correspondence with those of the total magnetic Gibbs free energy.[23] Thus the minimization of $W[\boldsymbol{J}_s, \boldsymbol{A}]$ with respect to $\boldsymbol{J}_s$ and $\boldsymbol{A}$ provides a stable equilibrium state and makes $\boldsymbol{A}$ equal to the actual magnetic vector potential $\nabla\times\boldsymbol{A} = \mu_0\boldsymbol{H}_s + \boldsymbol{J}_s$. Asselin and Thiele[23] proved that this method is also correct for two-dimensional geometries. If the magnetic particle has the shape of an infinite cylinder, the spontaneous magnetic polarization and the demagnetizing field depend only on two Cartesian coordinates, say x and y, and are independent of the third, z. Therefore the vector potential A reduces to a one-component potential, $\boldsymbol{A} = A(x,y)\hat{\boldsymbol{z}}$, where $\hat{\boldsymbol{z}}$ is the unit vector along the z direction. In two dimensions the auxiliary functional, which is obtained upon replacing the stray field energy in (2) by W_2, writes[23]

$$W[\boldsymbol{J}_s, A] = \int \left\{ A(\nabla\varphi)^2 + K_1\sin^2\varphi + K_2\sin^4\varphi - \boldsymbol{H}_{\text{ext}}\cdot\boldsymbol{J}_s \right\} d^2r + \frac{1}{2\mu_0}\int J_s^2\,d^2r - \frac{1}{\mu_0}\int \nabla A\cdot(\hat{\boldsymbol{z}}\times\boldsymbol{J}_s)\,d^2r + \frac{1}{2\mu_0}\int (\nabla A)^2\,d^2r. \tag{7}$$

The first integral over the magnetic body is the sum of the exchange energy, the crystalline anisotropy energy, and the magnetostatic energy. The following terms take care of the stray field energy.

Finite element calculations based on a vector potential formulation exhibit the following advantages over conventional numerical solutions of the micromagnetic problem: Since the functional $W[\boldsymbol{J}_s, A]$ depends only on local variables and their derivatives, its finite element discretization leads to a sparse matrix formulation of the micro-

magnetic problem. The problem is transformed into an algebraic minimization problem with respect to the two independent variables $\boldsymbol{J}_s$ and A. Thus convergence difficulties of iterative methods which are associated with a saddle-point principle can be avoided. Generally, it is easier to minimize a function than to search for a saddle point. Fredkin and Koehler[25] applied (7) in micromagnetic finite element calculations investigating magnetization processes in irregular shaped particles and systems of two particles. To discretize (7) they interpolated the potential linearily within each finite element and assumed the magnetization to be uniform in each element. Because the magnetization then is a piecewise constant function, the calculation of the exchange energy, which involves the gradient of the magnetization, is not straightforward. The ambiguity in evaluating the exchange energy can be avoided interpolating both the potential and the magnetization by linear functions within each element.[20] In contrast to the algorithm of Chen, Fredkin, and Koehler,[20] we use spherical coordinates and thus linearily interpolate the magnetization angle instead of the components of $\boldsymbol{J}_s$. This approach guarantees the magnitude of $\boldsymbol{J}_s$ to be constant over the entire ferromagnetic particle. The last integral in (7) is an integration over the whole space which can be evaluated using a spatial transformation.[26] In principle, the finite element mesh has to be extended over a large region outside the particle. Mapping the exterior region into a finite subdomain reduces the size of the external mesh and avoids the error associated with the truncation of the external mesh.

The repeated calculation of equilibrium states for decreasing external fields provides the demagnetization curve of the magnetic particles. In numerical micromagnetic calculations the inhomogeneous equilibrium states of the spontaneous magnetic polarization, $\boldsymbol{J}_s$, and the demagnetizing field, $\boldsymbol{H}_s$, lead to significant discretization errors.[27] In order to reduce these errors a mesh refinement procedure has been applied: The calculation is repeated on refined meshes, until the demagnetization curve is independent of the number of finite elements used.

III. GRAIN SIZE DEPENDENCE OF REMANENCE AND COERCIVITY

Figure 1 presents the microstructure used for the investigation of the grain size dependence of remanence and coercivity in nanocrystalline magnets. The particles of randomly oriented easy axes are coupled by direct exchange interactions and have hexagonal shape. For the calculations the material parameters of the $Fe_{14}Nd_2B$ phase at $T = 300$ K ($K_1 = 4.3\,10^6$ J/m^3, $K_2 = 0.65\,10^6$ J/m^3, $A = 7.7\,10^{-12}$ J/m, $J_s = 1.61$ T) (Ref. 28) have been used. The grain size has been varied between 10 nm and 60 nm.

Figure 2 shows the grain size dependence of the magnetic properties in isotropic nanocrystalline magnets. The numerically calculated values for the remanence and the coercive field are compared with experimental re-

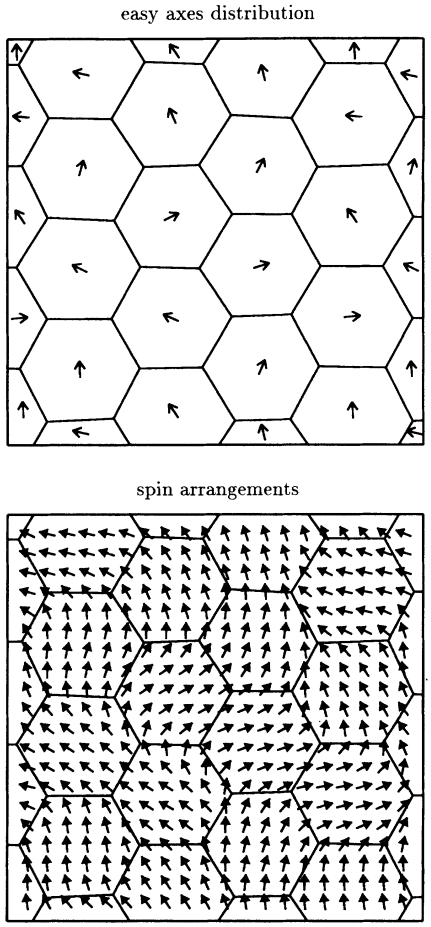

FIG. 1. Isotropic distribution of the easy axes and the corresponding spin arrangements for zero applied field. The grain diameter is 10 nm.

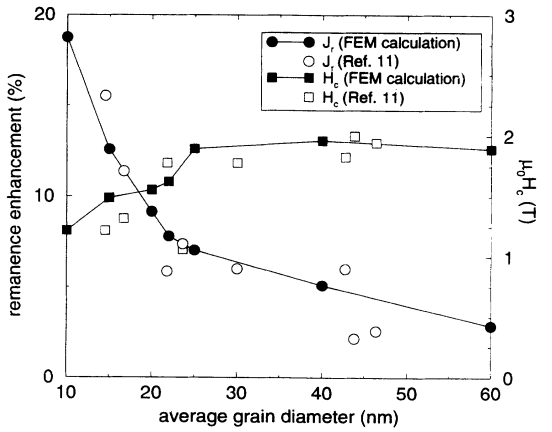

FIG. 2. Remanence and coercivity as a function of grain size. The remanence enhancement is given with respect to the theoretical limit for noninteracting particles. Circles, remanence enhancement; squares, coercive field. The open symbols refer to experimental values obtained for $Nd_{13.2}Fe_{79.6}B_6Si_{1.2}$ melt-spun ribbons (Ref. 11).

sults from Manaf *et al.*[11] obtained for $Nd_{13.2}Fe_{79.6}B_6Si_{1.2}$ melt-spun ribbons. Numerically calculated values are denoted by closed symbols, whereas experimental values are denoted by open symbols. To compare numerically calculated and experimental values of the remanence, we have to take into account the in-plane anisotropy inherent in the two-dimensional calculations. Therefore the plot shows only the enhancement of the remanence with respect to its value for noninteracting particles. Thus the circles in Fig. 2 refer to $100 \times J_r/(0.637J_s)$ for the numerically calculated and to $100 \times J_r/(0.5J_s)$ for the experimental values of the remanence.

Remanence increases with decreasing grain size. For a grain size $d < 20$ nm exchange interactions between the grains enhance the remanence by about 15% as compared to the remanent state of noninteracting particles. However, highly remanent magnets exhibit low coercive fields. Coercivity significantly decreases at a grain size of about 20 nm. The numerically obtained results for remanence and coercivity are in excellent agreement with the experimentally observed behavior.[11]

This relation between coercivity and remanence can be understood comparing the spin arrangements for zero applied field as function of grain size. Exchange interactions between neighboring grains account for the particular distribution of $\boldsymbol{J}_s$ in the remanent state, plotted in Fig. 1 for a grain size of 10 nm. After saturation by a large external field, the equilibrium states have been calculated for decreasing external field. As the external field drops, the magnetic polarization of each individual grain rotates towards its particular easy axis. However, in the remanent state the spontaneous magnetic polarization $\boldsymbol{J}_s$ was found to deviate from the easy axes in the vicinity of the grain boundaries. The competitive effects of magnetocrystalline anisotropy and exchange interaction cause a smooth transition of $\boldsymbol{J}_s$ from one easy axis direction to the other over a width of δ_B. As a consequence the resultant polarization parallel to the field direction is increased compared to the remanence of noninteracting particles. Figure 3 clearly demonstrates the dependence of high remanence effects on the mean grain size. The emphasized areas in Fig. 3 indicate the regions where $\boldsymbol{J}_s$ deviates from its local easy axes by more than 10° and 20°. The width of these inhomogeneous magnetic states along the grain boundaries is comparable with the domain wall with $\delta_B = \pi\sqrt{A/K_1}$. Only the magnetic moments within the boundary region where $\boldsymbol{J}_s$ deviates from the easy axes can increase the remanence. The volume fraction of the inhomogeneous magnetic state along the grain boundaries becomes larger for smaller grain size. Therefore remanence enhancement is more significant for smaller grains. The remanence of randomly oriented nanocrystalline particles which are strongly coupled by exchange interactions increases with decreasing grain size.

Furthermore, Fig. 3 reveals grains with almost all the spins deviating from the easy axis. Exchange interactions between neighboring grains override the magnetic anisotropy of the individual grains if the average grain diameter approaches the domain wall width. Owing to the strongly inhomogeneous ground state, the expense of exchange and anisotropy energy in the remanent state is remarkably high. Thus the system can obtain a significant gain in exchange and anisotropy energy, if magnetization reversal is initiated. The numerical calculations show that for a mean grain size of 15 nm the gain in exchange and anisotropy energy is three times larger than for a grain size of 40 nm. The strongly inhomogeneous magnetic ground state formed in small-grained microstructures favors the nucleation of reversed domains, because of the gain in exchange and crystalline anisotropy energy after magnetization reversal. Thus one can conclude that the deviation of the magnetic polarization from the easy direction near grain boundaries becomes the crucial effect which determines remanence and coercivity of nanocrystalline permanent magnets. However, it is not obvious whether these deviations are due to exchange or magnetostatic effects, avoiding poles at grain boundaries.

In order to separate the effects of exchange and magnetostatic interactions, reference calculations omitting either the stray field or the exchange terms in the total magnetic Gibbs free energy were performed. Figure 4 compares the demagnetization curves obtained taking

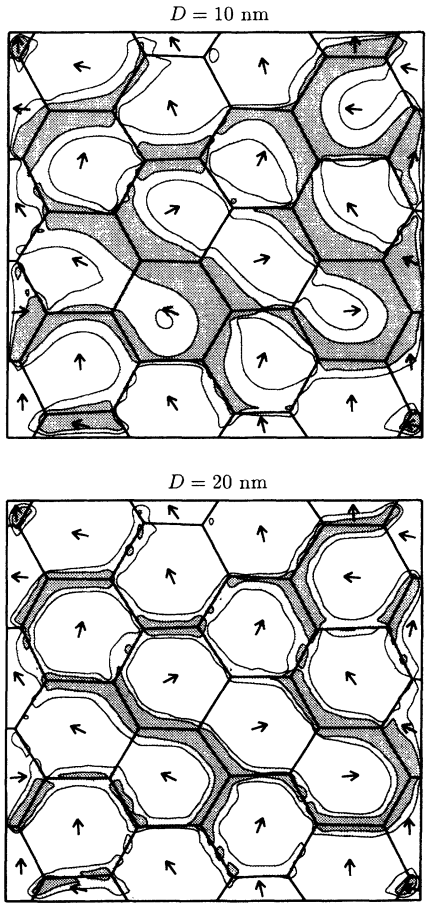

FIG. 3. Inhomogeneous regions along the grain boundaries. The arrows indicate the direction of the easy axes. The shaded areas denote the regions where the magnetic polarization deviates from the local easy axis by more than 10° and 20°, respectively.

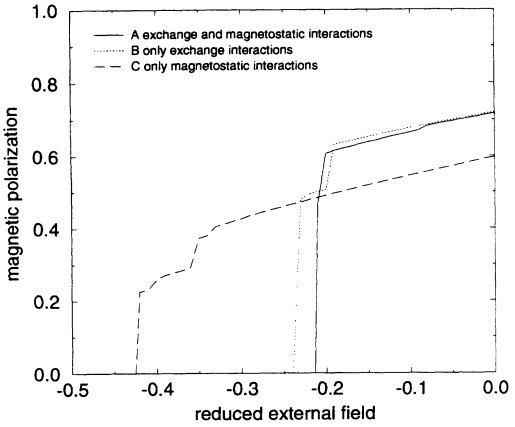

FIG. 4. Influence of exchange and magnetostatic interactions on the magnetic properties. The plots give the demagnetization curves of randomly oriented grains with a mean grain size of 15 nm, taking into account (A) exchange and magnetostatic interactions, (B) only exchange interactions, and (C) only magnetostatic interactions. The magnetic polarization normalized by its saturation value is plotted as a function of the external field. The external field is given in units of $2K_1/J_s$.

into account (A) exchange and magnetostatic interactions, (B) only exchange interactions, and (C) only magnetostatic interactions. The mean grain size was 15 nm so that we can expect a significant volume fraction of inhomogeneous magnetic states at the grain boundaries. For calculation (A) the remanence was $J_r/J_s = 0.72$ giving a remanence enhancement of 14%, whereas the coercive field reached only 22% of the ideal nucleation field, $2K_1/J_s$. The results merely change if magnetostatic interactions are neglected (B). A completely different behavior was found taking into account only magnetostatic interactions (C). Here the remanence decreases rather than increases as compared to the value of noninteracting particles. Remanence enhancement is only possible when a significant number of magnetic moments deviates from the easy axes. Therefore the deviations of the magnetic polarization from the easy direction near the grain boundaries have to be entirely attributed to exchange coupling of neighboring grains. Furthermore, the calculation shows that magnetostatic interactions do not significantly reduce the coercive field. The obtained value of the coercive field is close to the expected value, $H_c = 0.48 \times 2K_1/J_s$, for randomly oriented, noninteracting, spherical particles.[7] The slight additional reduction of the coercive field may be attributed to the macrosopic demagnetizing field of the cylindrical particle.

Numerical micromagnetic analyses clearly show that strong exchange interactions account for remanence enhancement and low coercivities in isotropic nanocrystalline permanent magnets. Long-range magnetostatic interactions play a minor role in the demagnetization reversal process of small-grained magnets with uniform grain structure. As discussed in the following section, demagnetizing fields become important for inhomogeneous microstructures with a large range in grain size and particle shape.

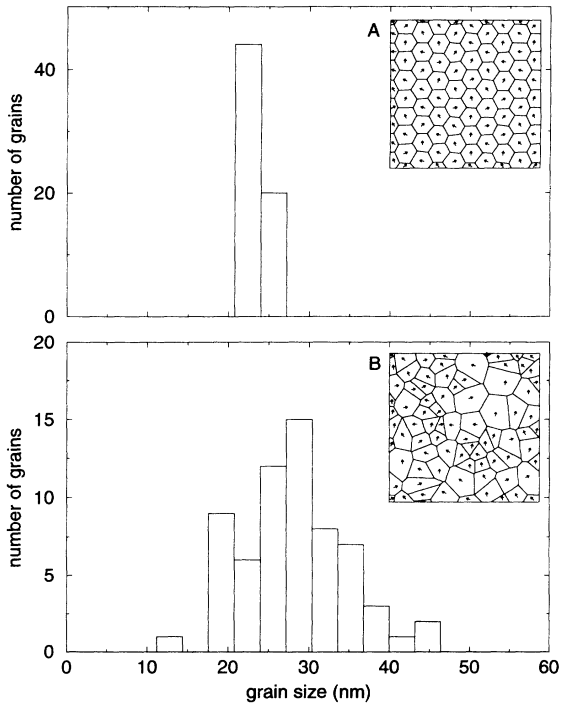

FIG. 5. Grain size distribution and the corresponding microstructures of the particle configurations used for the simulations of size and shape effects.

IV. THE EFFECT OF GRAIN SIZE DISTRIBUTION ON COERCIVITY

Figure 5 presents the grain size distributions of the particle configurations used for investigation of size and shape effects on the magnetic properties. The insets show the corresponding two-dimensional grain structures. The randomly oriented particles have direct exchange interactions. Whereas configuration A has a nearly uniform

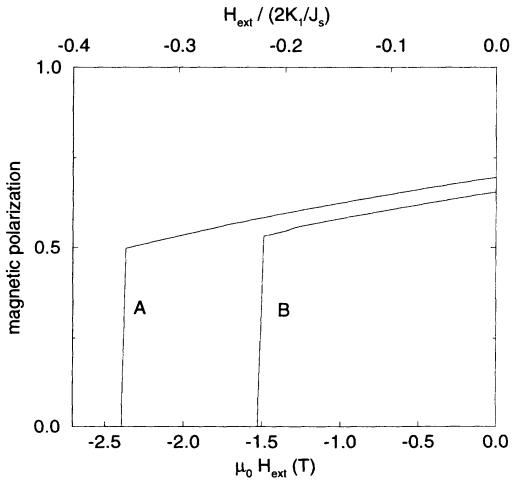

FIG. 6. Demagnetization curves for uniform grain structure (A) and inhomogeneous grain structure (B). The magnetic polarization normalized by its saturation value is plotted as a function of the external field. The external field is given in units of $2K_1/J_s$.

grain structure, the particles of configuration B drastically vary in size and shape. To build the grain structures, a model simulating the grain growth has been used:[29,30] Starting from randomly located seed points, grains grow with constant growth velocity in each direction. For the calculations the material parameters of the $Fe_{14}Nd_2B$ phase at $T = 300$ K have been used. The comparison of the demagnetization curves for the particle configurations A and B, given in Fig. 6, shows that both remanence and coercive field strongly depend on the microstructure.

In addition to short-range exchange coupling, long-range magnetostatic interactions between the grains considerably influence the magnetic behavior of permanent magnets. A significant contribution to the demagnetizing field arises from magnetic volume charges owing to inhomogeneous distributions of $\boldsymbol{J}_s$ along the grain boundaries. Therefore the strength and orientation of the demagnetizing field reflects the grain structure. Figures 7 and 8 give a comparison of the spin arrangements and the stray field of both microstructures for different applied fields. The plots show that the absolute value of the stray field reaches its maximum near grain boundary junctions of strongly misoriented grains. In the lower right quarter of microstructure B (see Fig. 8), where several small grains come together, the local demagnetization factor ($N_{\text{eff}} = \mu_0|H_s|/J_s$) for zero applied field was found to be as high as $N_{\text{eff}} = 1.6$. Whereas for microstructure A the local demagnetization factor for zero applied field reaches only values of $N_{\text{eff}} = 1.4$. The increased stray fields considerably reduce the coercivity of nanocrystalline magnets with inhomogeneous grain structure.

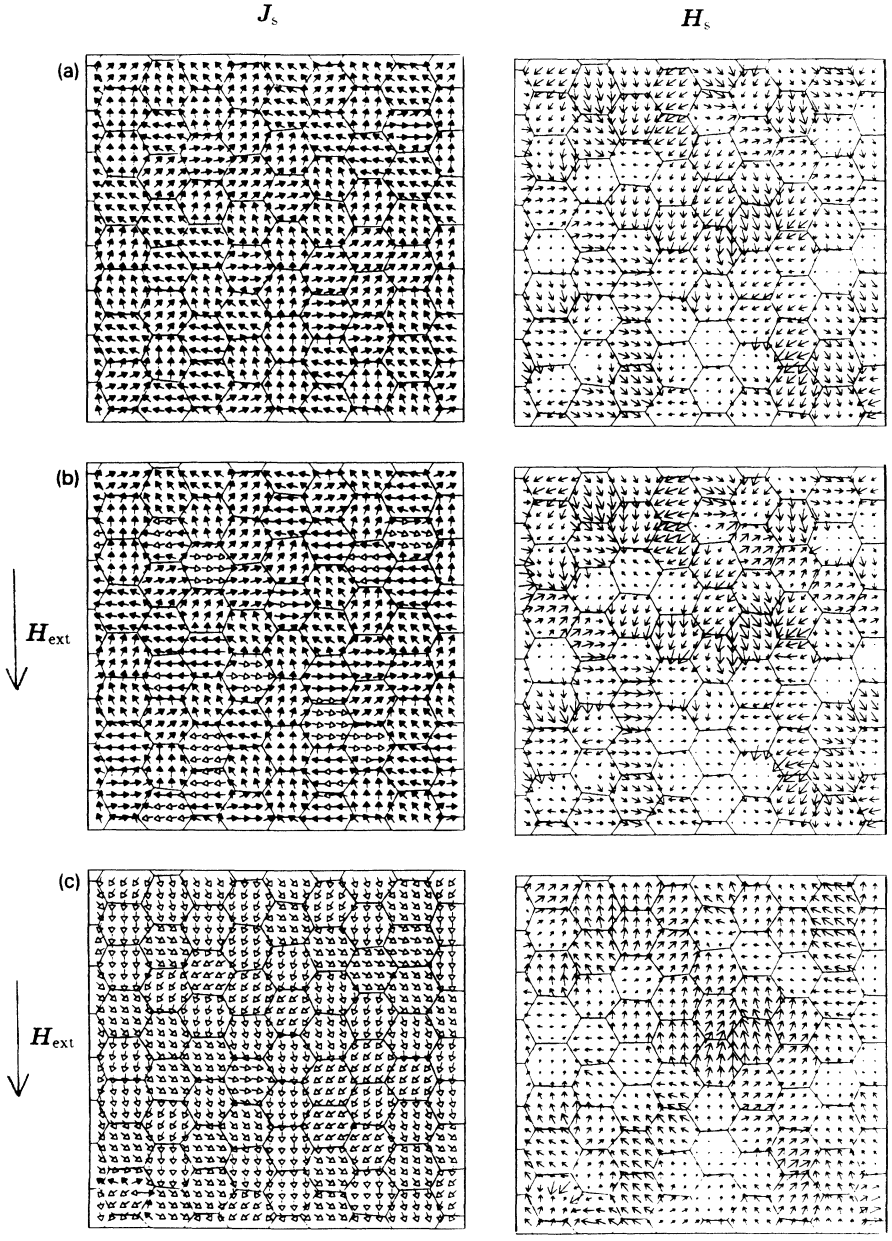

FIG. 7. Spin arrangements and demagnetizing field for different applied field for an isotropic nanocrystalline $Nd_2Fe_{14}B$ magnet with uniform grain structure (particle configuration A). Left-hand side: distribution of the spontaneous magnetic polarization. Right-hand side: direction and strength of the demagnetizing field. The length of the arrows indicates the absolute value of the demagnetizing field. (a) Remanent state $\mu_0 H_{\text{ext}} = 0$; (b) undercritical state $\mu_0 H_{\text{ext}} = 2.38$ T; (c) reversed magnetic state $\mu_0 H_{\text{ext}} = 2.39$ T.

V. MAGNETIC PROPERTIES OF TWO-PHASE PERMANENT MAGNETS

The demagnetization curves, presented in Fig. 9, show the magnetic properties of isotropic two-phase magnets for increasing volume fraction of the soft magnetic phase. The insets show the corresponding microstructures being composed of magnetically soft and hard grains. For the soft magnetic and hard magnetic phase the material parameters of α-Fe and $Fe_{14}Nd_2B$ at $T = 300$ K have been used, respectively (α-Fe: $K_1 = 4.6 \times 10^4$ J/m^3, $K_2 = 1.5 \times 10^4$ J/m^3, $A = 2.5 \times 10^{-11}$ J/m, $J_s = 2.15$ T).[31] In addition, Fig. 9 compares the demagnetization curve obtained for an average grain size of 10 nm and 20 nm. The results clearly show that a small grain size improves both remanence and coercivity of isotropic two-phase magnets. The spin arrangements for zero applied field, given in Figs. 10(a) and 10(b), demonstrate the effect of the particle size: For a grain size of 10 nm almost all the spins of the soft magnetic phase are aligned parallel to the direction of the applied field. For a grain size of 20 nm the range of exchange interactions, which couples the soft magnetic moments to the hard magnetic phase, is too short to align the soft magnetic grains completely. The magnetic properties summarized in Table I show that exchange interactions between hard and soft magnetic phases increase the ratio of remanent and saturation polarization up to $J_r/J_s = 0.92$.

For the calculations the hard magnetic grains have been randomly oriented fulfilling the condition

$$\frac{\sum a_i \cos \vartheta_i}{\sum a_i} = \frac{2}{\pi}, \tag{8}$$

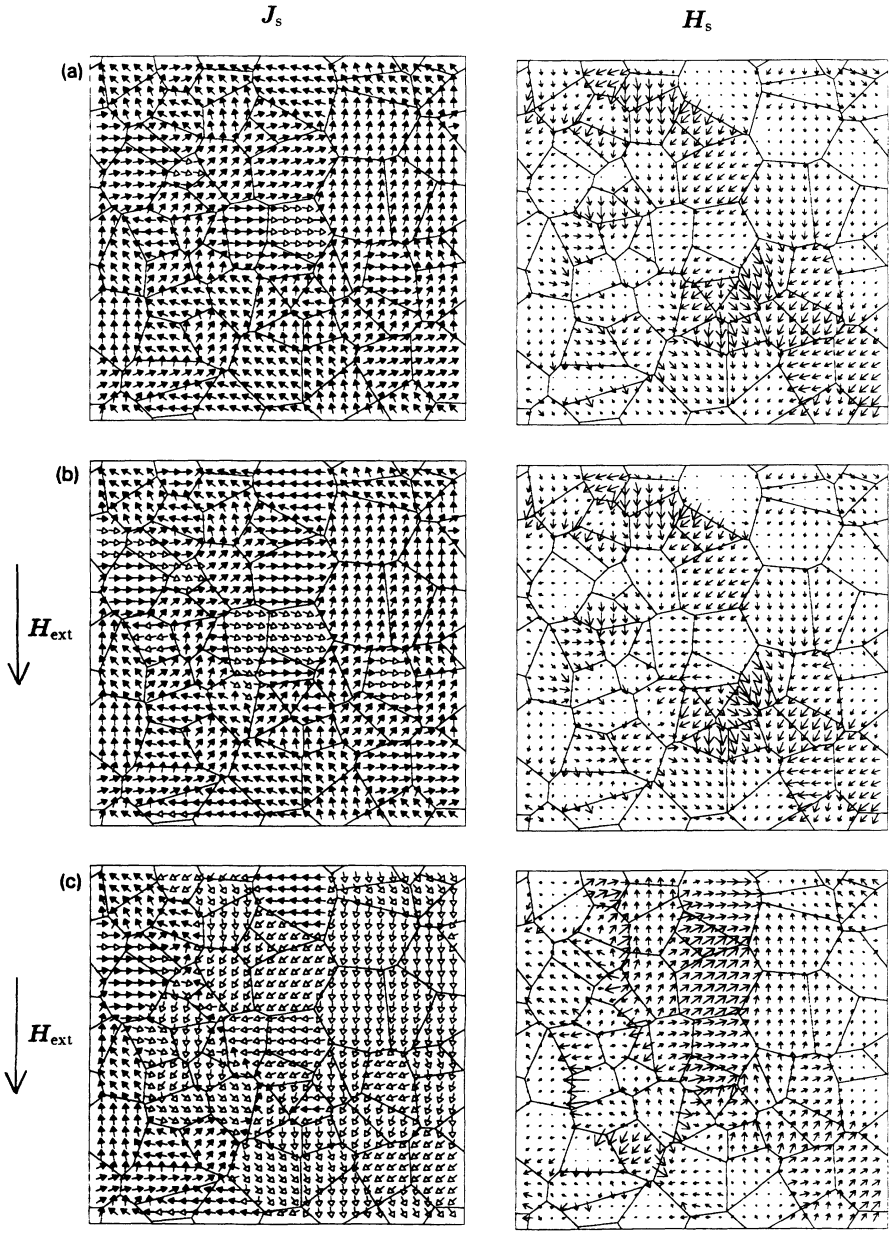

FIG. 8. Spin arrangements and demagnetizing field for different applied field for an isotropic nanocrystalline $Nd_2Fe_{14}B$ magnet with inhomogeneous grain structure (particle configuration B). Left-hand side: distribution of the spontaneous magnetic polarization. Right-hand side: direction and strength of the demagnetizing field. The length of the arrows indicates the absolute value of the demagnetizing field. (a) Remanent state $\mu_0 H_{ext} = 0$; (b) undercritical state $\mu_0 H_{ext} = 1.51$ T; (c) reversed magnetic state $\mu_0 H_{ext} = 1.52$ T.

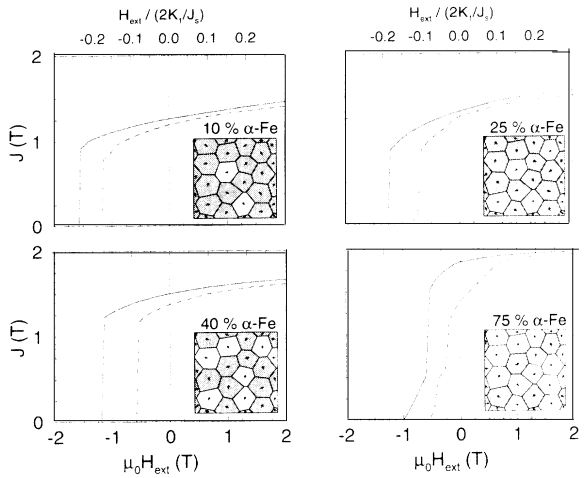

FIG. 9. Demagnetization curves of isotropic two-phase permanent magnets. The insets show the corresponding microstructures. The arrows indicate the direction of the easy axes. The open and shaded grains denote the soft and hard magnetic phases, respectively.

where a_i is the area of the hard magnetic grain i oriented under the angle ϑ_i with respect to the direction of the applied field. However, owing to the limited number of hard magnetic grains, remanence enhancement is expected to depend on the particular easy axes distribution assumed for the calculation, especially if the volume fraction of the hard phase is low. In order to give a quantitative treatment of this effect, the easy axes distribution has been varied systematically for the microstructure containing 25% $Fe_{14}Nd_2B$ and 75% α-Fe. These investigations of the influence of the easy axes distribution on the magnetic properties has been done for an average grain size of $d = 10$ nm. The maximum remanence enhancement of $J_r/J_s = 0.92$ was found for an easy axes distribution without any hard magnetic grains oriented perpendicular to the field direction. However, in real magnets there are always such grains. Therefore, for each following calculation one of the angles ϑ_i has been fixed to 90° with all the hard magnetic grains still fulfilling Eq. (8). The ratio of remanent and saturation polarization and the coercive field was found to vary with the easy axes distribution between $J_r/J_s = 0.92$ and $J_r/J_s = 0.66$ and between $\mu_0 H_c = 1.0$ T and $\mu_0 H_c = 0.55$ T, respectively. The configuration where the hard magnetic grain in the center of the microstructure is oriented perpendicular to the field direction exhibits the lowest value of the remanence. Figures 10(a) and 10(c) show the spin arrangements in the remanent state for the easy axes distributions exhibiting maximum and minimum remanence enhancement. The ratio of remanence to saturation polarization averaged over all configurations still shows a remarkable value of $J_r/J_s = 0.81$ for a volume fraction of the soft magnetic phase of 75% and a mean grain size of $d = 10$ nm. The last five rows of Table I give the magnetic properties obtained for different orientations of the hard magnetic grains for the microstructure with a mean grain size of $d = 10$ nm and a volume fraction of soft magnetic phases of 75%. In the following figures the magnetic properties of the microstructure for a volume fraction of 75% α-Fe and for a grain size of $d = 10$ nm denote the mean results obtained for the different orientations of the hard magnetic grains. The magnetic properties for a grain size of $d = 20$ nm have been calculated for the optimal distribution of the easy axes without any grains oriented perpendicalur to the field direction.

Figure 11 shows the remanence and the coercivity as a function of the volume fraction of the soft magnetic phase. The increase of the remanence with increasing number of magnetically soft grains is much more significant for smaller grains. In addition, coercivity remains

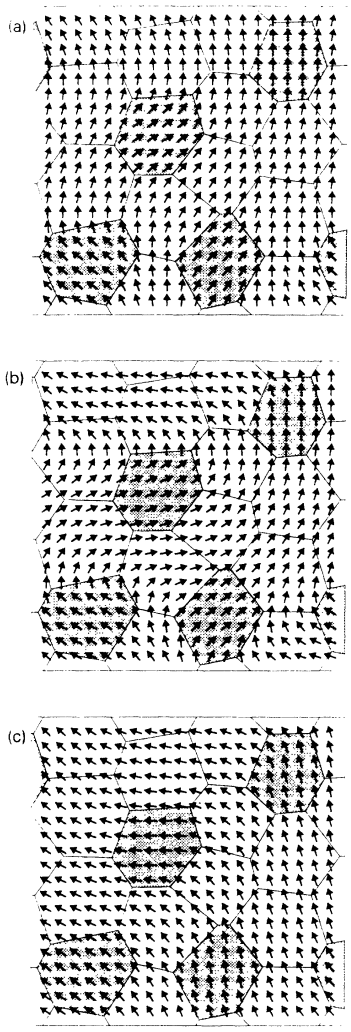

FIG. 10. Distribution of the spontaneous magnetic polarization in isotropic two-phase permanent magnets for zero applied field. The open and shaded grains denote the soft and hard magnetic phases, respectively. The volume fraction of the magnetically soft phase is 75%. (a) Mean grain size $D = 10$ nm, optimal distribution of the easy axes without any hard magnetic grain oriented perpendicular to the field direction: $J_r/J_s = 0.92$; (b) mean grain size $D = 20$ nm, optimal distribution of the easy axes: $J_r/J_s = 0.69$; (c) mean grain size $D = 10$ nm, easy axes distribution with the hard magnetic grain in the center oriented perpendicular to the field direction: $J_r/J_s = 0.66$.

TABLE I. Correlation between microstructural features and magnetic properties in isotropic nanocrystalline permanent magnets. The first four columns characterize the microstructures. The following columns give the numerical results for the remanence, the ratio of the remanent polarization J_r to the saturation polarization J_s, the nucleation field, the coercive field, and the maximum energy product. The nucleation field denotes the critical value of the external field where the spontaneous magnetic polarization rotates irreversibly. The last five rows give the magnetic properties of isotropic two-phase magnets for different distributions of the easy axes.

Number of grains	Mean grain size (nm)	Range in grain size (nm)	Soft magnetic phases (%)	J_r (T)	J_r/J_s	$\mu_0 H_N$ (T)	$\mu_0 H_c$ (T)	$(BH)_{max}$ (kJ/m^3)
16	10	0.5	0	1.22	0.76	1.22	1.75	287
16	15	0.75	0	1.15	0.72	1.44	1.44	258
16	20	1.0	0	1.12	0.70	1.52	1.52	237
16	25	1.25	0	1.10	0.68	1.92	1.92	233
16	40	2.0	0	1.08	0.67	1.92	1.92	224
16	60	3.0	0	1.05	0.65	1.85	1.85	212
64	24	3.5	0	1.12	0.70	2.39	2.39	243
64	29	32.0	0	1.06	0.66	1.52	1.52	215
16	20	5.0	10	1.19	0.71	1.19	1.19	272
16	20	5.0	25	1.10	0.63	0.91	0.91	304
16	20	5.0	40	1.37	0.76	0.59	0.59	361
16	20	5.0	75	1.39	0.69	0.27	0.57	345
16	10	2.5	10	1.26	0.76	1.59	1.59	308
16	10	2.5	25	1.21	0.70	1.37	1.37	338
16	10	2.5	40	1.50	0.83	1.21	1.21	439
16	10	2.5	75	1.85	0.92	0.61	1.01	662
16	10	2.5	75	1.79	0.88	0.57	0.57	616
16	10	2.5	75	1.66	0.82	0.90	0.90	523
16	10	2.5	75	1.57	0.78	0.54	0.60	460
16	10	2.5	75	1.33	0.66	0.20	0.55	280

remarkably high even for a volume fraction of the soft phase of 75%, if the grain size is 10 nm. Besides the increase of the remanence, a large number of magnetically soft phases avoids hard magnetic grains which are in direct contact. Thus the reduction of the coercive field owing to exchange interactions between misoriented hard magnetic grains can be suppressed. The remarkably high values of the coercive field of about 1 T, found for the optimally structured two-phase magnets, can be attributed to two micromagnetic effects: (1) Exchange hardening of a magnetically soft grain is effective, if the extension of the magnetically soft phase is smaller than twice the domain wall width of the hard phase.[32] (2) Exchange interactions between hard magnetic grains, which decrease coercivity, are avoided.

Because it is possible to increase the remanence while preserving a high coercive field, isotropic two-phase permanent magnets with an optimal microstructure exhibit remarkable high-energy products. Figure 12 gives the numerically calculated maximum energy product as a function of the volume fraction of the soft magnetic phase for 10 nm and 20 nm grain size. For a grain size of 10 nm and a volume fraction of the soft magnetic phase of 75% the maximum energy product exceeds 500 kJ/m^3. For a large grain size remanence as well as coercivity decrease, if the volume fraction of the soft magnetic phase becomes too high. Nevertheless, two-phase permanent magnets with a grain size of 20 nm still exhibit a maximum energy product of about 350 kJ/m^3 for a volume fraction of the soft magnetic phase of 40%. For the calculation of the energy products the demagnetization curves have been

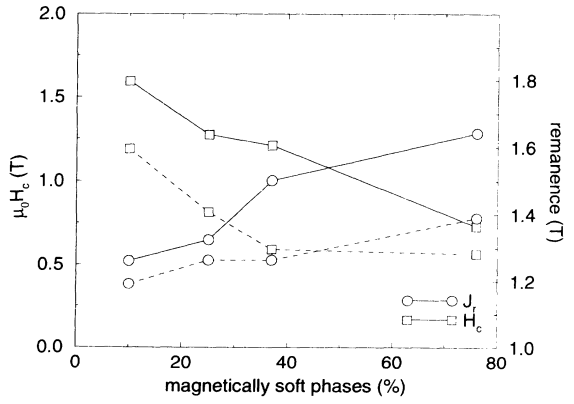

FIG. 11. Remanence and coercivity of two-phase permanent magnets as a function of the volume fraction of magnetically soft phases. (o—o) remanent polarization for a grain size of 10 nm. (o – –o) remanent polarization for a grain size of 20 nm. (□—□) coercive field for a grain size of 10 nm. (□ – –□) coercive field for a grain size of 20 nm.

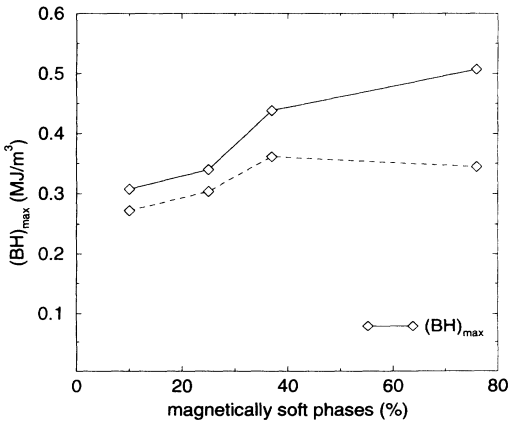

FIG. 12. Maximum energy product of two-phase permanent magnets as a function of the volume fraction of magnetically soft phases. (◇—◇) $(BH)_{max}$ for a grain size of 10 nm. (◇ – –◇) $(BH)_{max}$ for a grain size of 20 nm.

corrected assuming a demagnetization factor, $N = 1/2$, of a cylindrical particle. Because of in-plane anisotropy in two-dimensional calculations the numerically obtained energy products are probably overestimated.

VI. CONCLUSION

The numerical results summarized in Table I show that the magnetic properties of isotropic nanostructured permanent magnets are extremely sensitive to the microstructure. Numerical micromagnetic calculations provide the following guidelines to optimize the microstructure of nanocrystalline permanent magnets.

(1) In order to achieve a significant enhancement of the remanence and to preserve a high coercive field in isotropic nanocrystalline $Fe_{14}Nd_2B$-based magnets, a mean grain size $d < 20$ nm and a homogeneous microstructure with a very small range in grain size are required.

(2) In isotropic two-phase magnets a small average grain size improves the remanence as well as the coercive field. For a grain size of about twice the domain wall width of the hard phase, the volume fraction of the magnetically soft phase can be increased up to 50% without a significant reduction of the coercive field.

[1] E. F. Kneller and R. Hawig, IEEE Trans. Magn. **27**, 3588 (1991).
[2] R. W. McCallum, A. M. Kadin, G. B. Clemente, and J. E. Keem, J. Appl. Phys. **61**, 3577 (1987).
[3] R. Coehoorn, D. B. Mooij, and C. D. E. Waard, J. Magn. Magn. Mater. **80**, 101 (1989).
[4] J. Ding, P. G. McCormick, and R. Street, J. Magn. Magn. Mater. **124**, 1 (1993).
[5] G. B. Clemente, J. E. Keem, and J. P. Bradley, J. Appl. Phys. **64**, 5299 (1988).
[6] G. C. Hadjipanayis and W. Gong, J. Appl. Phys. **64**, 5559 (1988).
[7] E. C. Stoner and E. P. Wohlfarth, Philos. Trans. R. Soc. **240**, 599 (1948).
[8] M. G. Grönefeld, Ph.D. thesis, University of Stuttgart, Germany, 1990.
[9] A. Hernando, I. Navarro, and J. M. Gonzáles, Europhys. Lett. **20**, 175 (1992).
[10] T. Schrefl, H. F. Schmidts, J. Fidler, and H. Kronmüller, J. Magn. Magn. Mater. **124**, 251 (1993).
[11] A. Manaf, R. A. Buckley, H. A. Davies, and M. Leonowicz, J. Magn. Magn. Mater. **101**, 360 (1991).
[12] E. Callen, Y. J. Liu, and J. R. Cullen, Phys. Rev. B **16**, 263 (1977).
[13] H. Fukunaga and H. Inoue, Jpn. J. Appl. Phys. **31**, 1347 (1992).
[14] S. Nieber and H. Kronmüller, Phys. Status Solidi B **153**, 367 (1989).
[15] R. Skomski and J. M. D. Coey, IEEE Trans. Magn. (to be published).
[16] T. Schrefl, Ph.D. thesis, Technical University Vienna, Vienna, 1993.
[17] H. Kronmüller, Phys. Status Solidi B **144**, 385 (1987).
[18] H. Kronmüller, K. D. Durst, S. Hock, and G. Martinek, J. Phys. Paris (Colloq.) **49**, C8-623 (1988).
[19] T. R. Koehler and D. R. Fredkin, IEEE Trans. Magn. **28**, 1239 (1992).
[20] W. Chen, D. R. Fredkin, and T. R. Koehler, IEEE Trans. Magn. **29**, 2124 (1993).
[21] H. F. Schmidts and H. Kronmüller, J. Magn. Magn. Mater. **94**, 220 (1991).
[22] W. F. Brown, Jr., J. Phys. Soc. Jpn. Suppl. B-I **17**, 540 (1962).
[23] P. Asselin and A. A. Thiele, IEEE Trans. Magn. **22**, 1876 (1986).
[24] W. Döring, in *Handbuch der Physik*, edited by S. Flügge (Springer, Berlin, 1966), Vol. XVII/2.
[25] D. R. Fredkin and T. R. Koehler, IEEE Trans. Magn. **23**, 3385 (1987).
[26] X. Brunotte, G. Meunier, and J. F. Imhoff, IEEE Trans. Magn. **28**, 1663 (1992).
[27] Y. D. Yan and E. Della Torre, IEEE Trans. Magn. **24**, 2368 (1988).
[28] S. Hock, Ph.D. thesis, University of Stuttgart, Germany, 1988.
[29] Y. Otani, H. Li, and J. M. D. Coey, IEEE Trans. Magn. **26**, 2658 (1990).
[30] T. Schrefl and J. Fidler, J. Magn. Magn. Mater. **111**, 105 (1992).
[31] E. Kneller, *Ferromagnetismus* (Springer, Berlin, 1962).
[32] T. Schrefl, H. Kronmüller, and J. Fidler, J. Magn. Magn. Mater. **127**, L273 (1993).

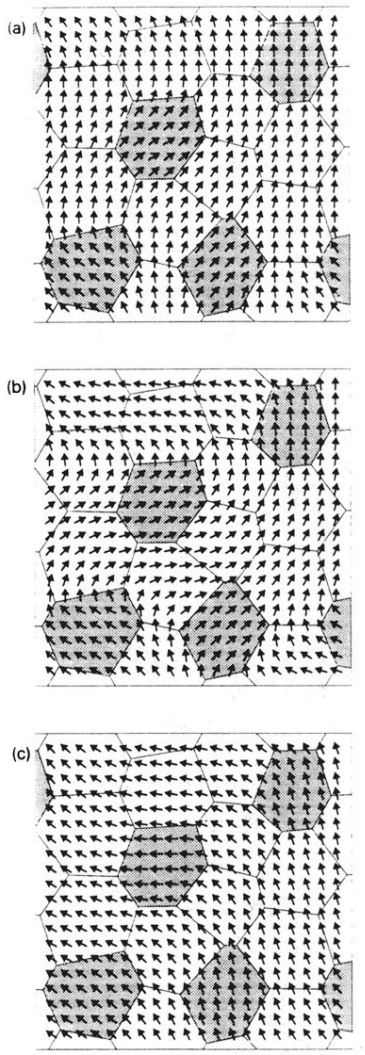

FIG. 10. Distribution of the spontaneous magnetic polarization in isotropic two-phase permanent magnets for zero applied field. The open and shaded grains denote the soft and hard magnetic phases, respectively. The volume fraction of the magnetically soft phase is 75%. (a) Mean grain size $D = 10$ nm, optimal distribution of the easy axes without any hard magnetic grain oriented perpendicular to the field direction: $J_r/J_s = 0.92$; (b) mean grain size $D = 20$ nm, optimal distribution of the easy axes: $J_r/J_s = 0.69$; (c) mean grain size $D = 10$ nm, easy axes distribution with the hard magnetic grain in the center oriented perpendicular to the field direction: $J_r/J_s = 0.66$.

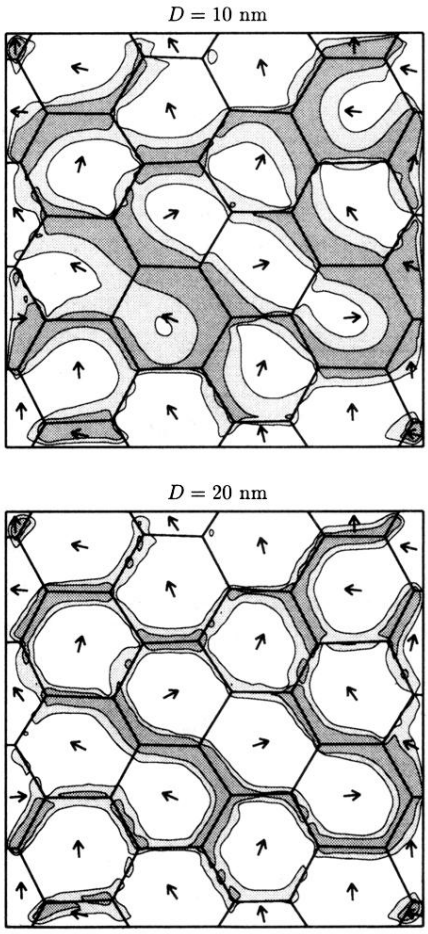

FIG. 3. Inhomogeneous regions along the grain boundaries. The arrows indicate the direction of the easy axes. The shaded areas denote the regions where the magnetic polarization deviates from the local easy axis by more than 10° and 20°, respectively.

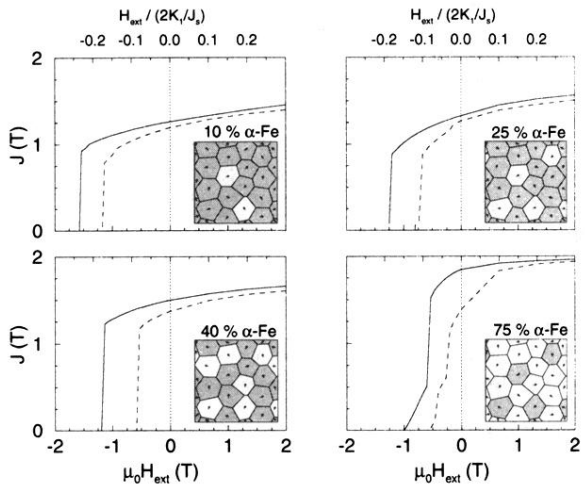

FIG. 9. Demagnetization curves of isotropic two-phase permanent magnets. The insets show the corresponding microstructures. The arrows indicate the direction of the easy axes. The open and shaded grains denote the soft and hard magnetic phases, respectively.